ISSN: 0256-307X

中国物理快报

Chinese Physics Letters

Volume 26 Number 9 September 2009

A Series Journal of the Chinese Physical Society
Distributed by IOP Publishing

Online: http://www.iop.org/journals/cpl
http://cpl.iphy.ac.cn

CHINESE PHYSICAL SOCIETY

CHIN. PHYS. LETT. Vol. 26, No. 9 (2009) 094701

Acoustic Calculation for Supersonic Turbulent Boundary Layer Flow *

LI Xin-Liang(李新亮)**, FU De-Xun(傅德薰), MA Yan-Wen(马延文), GAO Hui(高慧)
LNM, Institute of Mechanics, Chinese Academy of Sciences, Beijing 100190

(Received 19 May 2009)

An approach which combines direct numerical simulation (DNS) with the Lighthill acoustic analogy theory is used to study the potential noise sources during the transition process of a Mach 2.25 flat plate boundary layer. The quadrupole sound sources due to the flow fluctuations and the dipole sound sources due to the fluctuating surface stress are obtained. Numerical results suggest that formation of the high shear layers leads to a dramatic amplification of amplitude of the fluctuating quadrupole sound sources. Compared with the quadrupole sound source, the energy of dipole sound source is concentrated in the relatively low frequency range.

PACS: 47.27.Sd, 47.27.Ek, 47.27.Nb

Supersonic boundary layer transition flows are potential noise sources for flying vehicles. Therefore, a clear understanding of the sound source mechanisms associated with unsteady flow dynamics during the boundary layer flow transition is of great importance in the aerodynamic sound control of the flying vehicles. With the development of supercomputers, numerical simulation is playing a more and more important role in the study of sound radiation from turbulent flows (see Ref. [1] for a review). Since the sound energy is often several orders less than the kinetic energy of a fluid, it is not easy to compute the sound radiation directly without pollution by numerical error. Then, acoustic analogy theory[2] is usually used. Acoustic generation by transition fluids for incompressible flow has been studied by Wang *et al.*[3] by using the Lighthill acoustic analogy theory[2] based on the unsteady flow from direct numerical simulation (DNS). The acoustic calculations were focused on the quadrupole source functions. Compared with the quadrupole sound source, the dipole sound sources related to the wall boundary are more complex. In Curl's solution[4] to the Lighthill equation, both wall pressure and wall shear stress appear in the dipole sound source's integral expression. Then the dipole source related to the wall pressure is often called the "left dipole", because it is related to the left force of the body. However, as pointed out by Powell,[5] wall pressure is not a true sound source in the inviscous flow, but represents the effects of image quadrupoles. This conclusion is not strictly true for viscous flow, whereas it is approximately true in the boundary layer flow because $\partial p'/\partial n = 0$ holds approximately in the wall. Besides wall pressure, the role of wall shear stress to the sound source is still a source of argument. To clarify whether the wall shear can indeed be a valid sound source, Shariff *et al.*[6] directly computed the sound radiation from a tangential oscillating wall by solving compressible Navier–Stokes equations, and compared these results with the result of the Lighthill analogy theory. The study of Shariff *et al.* shows that the unsteady wall shear stress is a valid source of sound radiation. Hu *et al.*[7] have studied the sound radiation from a turbulent incompressible channel flow by using sound analogy theory and using the flow database from DNS as the source terms. Their radiation pressure spectrum agrees well with the experimental data[8] in higher frequencies, but about 15dB higher than the experimental spectrum in low frequencies.

Most studies on sound radiation from turbulent boundary layers are based on incompressible or low-Mach-number flows, and the study of supersonic or hypersonic boundary layer sound radiation is relatively few. As a typical turbulent boundary-layer case, the DNS of spatially evolving compressible flat-plate boundary layer flows with $M_\infty = 2.25$ and $Re = 635000/\text{inch}$ has been performed by Rai *et al.*,[9] Pirozzoli *et al.*[10] and Gao *et al.*[11] In this study, a new DNS with the same flow condition is performed to study the sound radiation. Compared with the original DNS,[11] the current DNS is carefully designed using higher mesh resolution, less dissipative and less dispersive numerical methods under better outlet boundary conditions with less artificial disturbance. Based on the present DNS results, the quadrupole and dipole sound sources produced in the process of transitions are studied by using the Lighthill acoustic analogy theory. The relationship between the sound source and high shear layers is studied, and the frequency spectra of the quadrupole and the dipole sound source are also analyzed.

The physical model is a spatially evolving compressible turbulent flat-plate boundary layer with $M_\infty = 2.25$ and $Re = 635000/\text{inch}$, and an imposed bow-and-suction perturbation is used to trigger the bypass transition. Details of this flow can be found in Refs. [9–11]. In this DNS, the compressible Navier–Stokes equations are solved numerically by using the WENO-SYMBO method with limter[12] for convection terms together with a eighth-order accurate central different for the viscous terms. A three-

*Supported by the National Natural Science Foundation of China under Grant Nos 10872205 and 10632050, and the National Basic Research Program of China under Grant No 2009CB724100.
**Email: lixl@lnm.imech.ac.cn

step TVD type Runge–Kutta method is used for time march. WENO-SYMBO[13] is a bandwidth optimized WENO scheme in the stencil of an eighth-order central scheme and its dissipation is further restrained by using limiters.[12] This scheme shows very low dissipation features in a DNS test for shock-turbulent-boundary-layer interaction.[12]

The three-dimensional computational domain consists of $4.0 \leq x \leq 9.6$ in the streamwise direction; $0 \leq y \leq 0.2$ in the wall normal direction, and $0 \leq z \leq 0.175$ inch in the spanwise direction. In this work, unless otherwise specified, all lengths are in inches. The flow and grid parameters are shown in Table 1. Compared with the authors' original DNS,[11] the grid number of the current DNS is increased to 2.5 times, and the spanwise computational domain is reduced to one-half ($Lz = 0.175$, the same as that in Ref. [10]), therefore the numerical resolution is much improved.

In order to obtain the inflow boundary conditions and initial conditions for the three-dimensional computation, a steady computation of two-dimensional laminar compressible flat-plate boundary layer flow including the leading-edge is carried out by using the same numerical method. The computed two-dimensional results at $x = 4.0$ inch are used as the inflow boundary conditions for the three-dimensional computation. Non-reflecting boundary conditions are used on the normal upper boundary and the downstream boundary. The non-slip and isothermal condition with constant wall temperature $T = T_w$ are used on the wall. In order to trigger the transition, a periodic blowing and suction disturbance on the upstream local wall ($4.5 \leq x \leq 5.0$) is imposed, and details of the imposed disturbance can be found in Refs. [9–11].

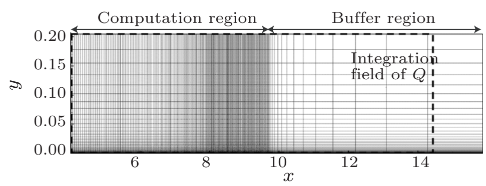

Fig. 1. Schematic of the computational domain, mesh and the integration field of Q.

Figure 1 shows the schematic of the computational domain and mesh. Concentrated meshes are used in the full turbulent region $8.0 \leq x \leq 9.6$ to obtain the best turbulence statistics. Gradually coarser meshes are used at $x > 9.6$ as a buffer region to minimize the numerical error generated by the outlet boundary condition. The numerical refraction of the outlet boundary is dissipated in the buffer region and has little effect to the computation region $x \leq 9.6$. The integration field of Q (sound source) is also shown in Fig. 1 by the dashed line. The outlet boundary of the integration field is set in the buffer region, which is helpful to minimize the artificial sound generated by the outlet boundary.[3] Flow and grid parameters are shown in Table 1. In the current DNS, a total of 40 million meshes are used, which is approximately 2.5 times the mesh number of our previous DNS.[11]

Table 1. Flow and grid parameters.

Re (inch)	635000
Ma_∞	2.25
T_w	1.9
Mesh number ($x \times y \times z$)	$2193 \times 72 \times 256$
$\Delta x^+ \times \Delta y_w^+ \times \Delta z^+$	$14.1 \times 1.1 \times 6.6$

Figure 2 shows the distribution of skin fraction coefficient C_f,[10] and the fast increase of C_f denotes the occurrence of transition. The theoretical value predicted by the Blasisus turbulence equation based on the momentous thickness and Van Dirst II transform[10] is also given in this figure. Figure 2 shows that our DNS results agree very well with the theoretical values.

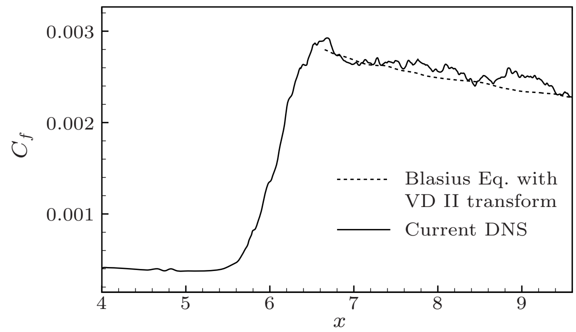

Fig. 2. Distribution of skin fraction coefficient.

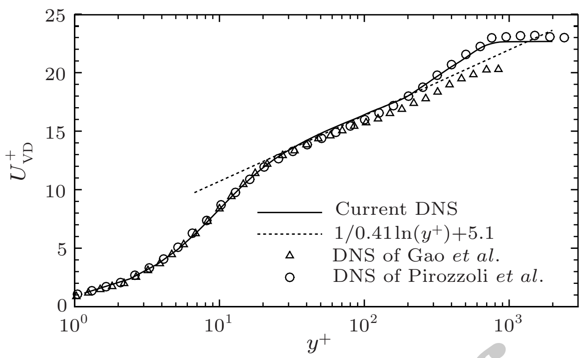

Fig. 3. Mean velocity profile normalized by wall shear velocity ($x = 8.8$ inch).

Figure 3 shows the mean Van Dirst velocity[10] profiles normalized by the wall-shear velocity at $x = 8.8$ results in the current DNS. This figure shows that the current results agree very well with the results of Pirozzoli *et al.*[10] which validates the current results. This figure also shows that the current DNS have higher resolution than our previous DNS.[11]

The contours of the spanwise vorticity in the (x, y) plane with $z = 0.0875$ at different times are shown in Fig. 4. This figure shows that high shear layers appear at $t = 3.0$ in the region $5.5 \leq x \leq 6.7$. The spanwise vorticity in the high shear layer is much higher (about 3–5 times) than the environment flow. Then the high shear layers go downsteam and become unstable. The instability of this high-shear layer leads

to laminar breakdown.

The above transition description shows that the transition process of the supersonic flat-plate boundary layer flow under the present conditions is the process which skips the T-S and second instability through the instability of the high gradient shear layer and leads to laminar breakdown. It means that the transition process is a bypass type transition process.

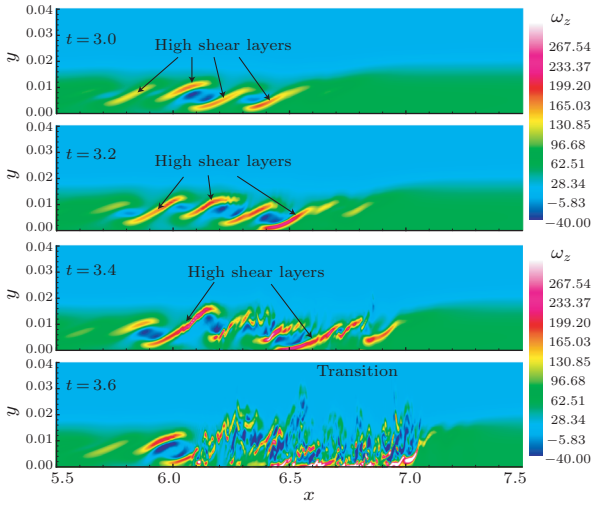

Fig. 4. Contours of the spanwise vorticity on the plane of (x, y) at $z = 0.00875$ at different times.

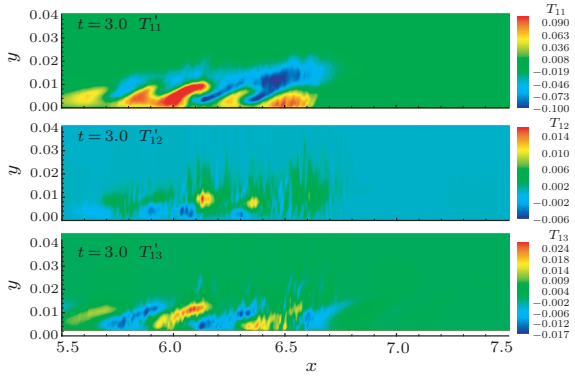

Fig. 5. Instantaneous contours of Lighthill stress fluctuation T'_{ij} at $t = 3.0$.

According to the Lighthill acoustic analogy theory, the fluctuating quadrupole sound sources obtained from Reynolds stress fluctuation can be written as[3]

$$\ddot{Q}_{ij} = \frac{\partial^2}{\partial t^2} \int_V T_{ij}(\boldsymbol{y}, t) d^3\boldsymbol{y}, \tag{1}$$

where

$$T_{ij} = \rho(u_i - U_i)(u_j - U_j) + \frac{\delta_{ij}}{M^2}\left(\frac{p}{\gamma} - \rho\right) - \tau_{ij},$$

is the Lighthill stress tensor. V denotes the integration field (see Fig. 1), and U_j denotes the free stream velocity. In our DNS the integration field is $4.0 \le x \le x_B$, here $x_B = 14.14$.

The dipole sound sources arising from the fluctuating surface stress of the flat plate are

$$\dot{D}_i = \frac{\partial}{\partial t} \int_S n_j \tau_{ij}(\boldsymbol{r}, t) dS, \tag{2}$$

where n_j denotes the normal vector of the surface S; $\tau_{ij} = \frac{\mu}{Re}\left(\frac{\partial u_i}{\partial x_j} + \frac{\partial u_j}{\partial x_i} - \frac{2}{3}\delta_{ij}\frac{\partial u_k}{\partial x_k}\right)$ is the shear stress tensor; S denotes the wall in the region $4.0 \le x \le x_B$.

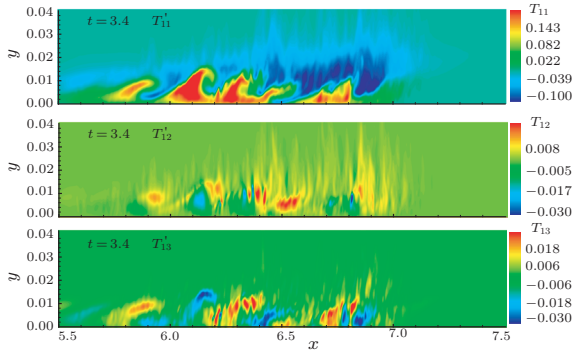

Fig. 6. Instantaneous contours of Lighthill stress fluctuation T'_{ij} at $t = 3.4$.

In order to eliminate the non-physical boundary effects which are produced when vortical structures pass out of the computational domain in the calculation of sound sources, the corrective formula derived by Wang *et al.*[3] is used. Denote $\ddot{Q}'_{ij}$ as the modified quadrupole sound source with the corrective formula which is expressed as

$$\ddot{Q}'_{ij} = \ddot{Q}_{ij} + \dot{F}_{ij}, \ \dot{F}_{ij} = \int_E u_1^B T_{ij} d^2 y, \tag{3}$$

where E denotes the downstream boundary plane of the integration field (see Fig. 1), and u_1^B is the streamwise velocity on this plane. The downstream boundary of the integration field is set in the buffer region (see Fig. 1). Since the flow fluctuation is very weak in the buffer region due to strong dissipation, artificial sound due to the downstream boundary is not strong and is easily removed using Eq. (3).

Instantaneous contours of the Lighthill stress fluctuation T'_{11} , T'_{12} and T'_{13} on the (x, y) plane at $z = 0.00875$ and at $t = 3.0$ and 3.4 are shown in Figs. 5 and 6, respectively. Here $T'_{ij} = T_{ij} - \bar{T}_{ij}$, and $\bar{T}_{ij}$ is the spanwise averaged Lighthill stress. Compared with Fig. 4, we can find that high-shear-layer regions are also high-Lighthill-stress regions, i.e. there is a clear correlation between a high-shear-layer and a high-Lighthill-stress region. This means that a high-shear layer is an important sound source.

Figure 7 shows the time history of the modified quadrupole sound source $\ddot{Q}'_{11}$ and the dipole sound source $\dot{D}_1$. It can be seen that both quadrupole and dipole sound sources are very weak at time $t < 3.0$. The amplitudes of $\ddot{Q}'_{11}$ and $\dot{D}_1$ increase suddenly during $3 \le t \le 3.8$ and become statistically steady at $t > 4$. Compared with Fig. 4, we can see that the time of sudden increase of the sound source is just the time

of the high shear layer breakdown. Thus there must be a strong relationship between the sound source and high shear layers.

Fourier spectrum analyses based on the time serial ($t \geq 4$) of $\ddot{Q}'_{ij}$ and $\dot{D}_j$ are performed. Figures 7 and 8 show the frequency spectrum of the quadrupole sound source $\ddot{Q}'_{ij}$ and dipole sound source $\dot{D}_j$, respectively. The frequency spectra of the quadrupole sound source $\ddot{Q}'_{ij}$ are wide-band spectra, which are typical characters of the turbulent flow. However, the frequency spectra of the dipole sound source $\dot{D}_j$ decays very fast in the high frequency region, and most energy is concentrated in the low-frequency region ($f \leq 30$). Figure 8 shows that the streamwise dipole $\dot{D}_1$ is much stronger than the spanwise dipole $\dot{D}_3$, and the wall-normal dipole $\dot{D}_2$ is the weakest one. According to Eq. (2), it can be deduced that wall shear stress τ_{xy} has the largest contribution to the dipole sound, and τ_{yy} has the lest contribution to the dipole sound. Since $\tau_{yy} = 4/3\nabla \cdot \boldsymbol{V}$ on the wall, this means that dilatation has little contribution to the wall dipole sound source.

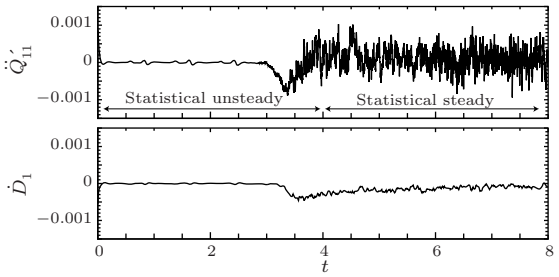

Fig. 7. Time history of modified quadrupole sound source $\ddot{Q}'_{11}$ and the dipole sound source $\dot{D}_1$.

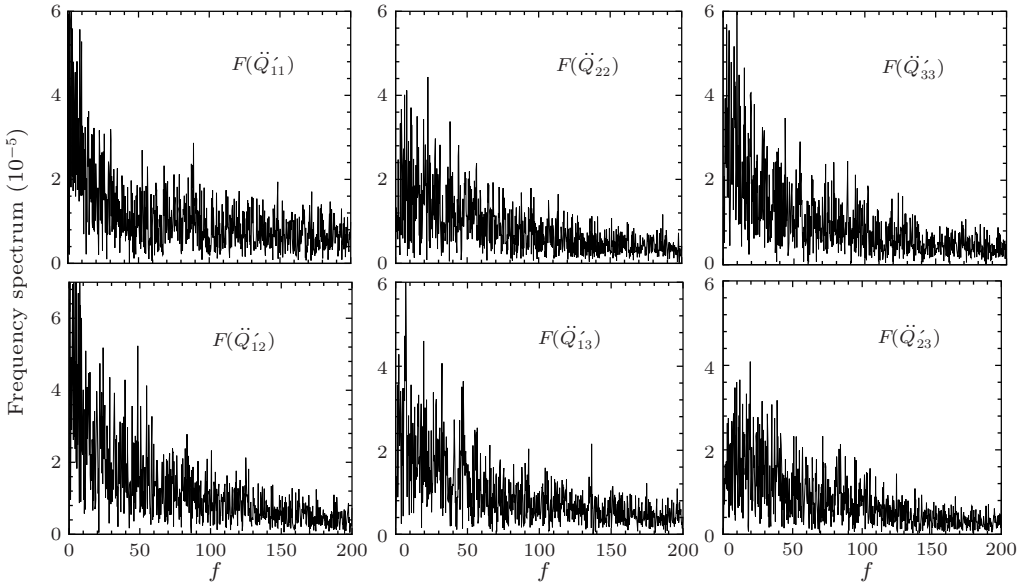

Fig. 8. Frequency spectra of the quadrupole sound sources.

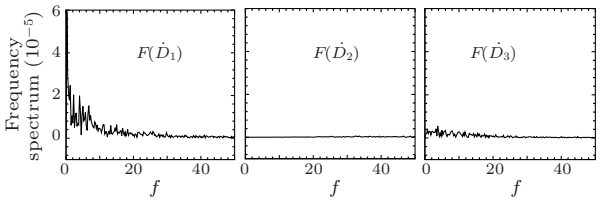

Fig. 9. Frequency spectra of the dipole sound sources.

In summary, we have carried out a direct numerical simulation (DNS) of spatially evolving compressible flat-plate boundary layer flow with free-stream Mach number $M_\infty = 2.25$ and Reynolds number $Re = 635000$/inch. The result is well validated by compararison with theoretical and other numerical results. Based on the DNS data and Lighthill's acoustic analogy theory, the quadrupole sound source due to the inner flow and dipole sound source due to the wall shear stress is computed and analyzed. The instability of high shear layers are important quadrupole sound sources. The energy of the dipole sound source is concentrated in the low-frequency range, and its character frequency is much lower than the quadrupole sound source. Shear stress τ_{xy} has the most important contribution to the dipole sound source, and the contribution of τ_{yz} to the dipole sound source is relatively weak. Dilatation has little contribution to the dipole sound source.

References

[1] Wang M et al 2006 *Ann. Rev. Fluid Mech.* **38** 483
[2] Lighthill M J 1952 *Proc. R. Soc. London A* **211** 564
[3] Wang M et al 1996 *J. Fluid Mech.* **319** 197
[4] Curle N 1955 *Proc. R. Soc. London* A **231** 505
[5] Powell A 1960 *J. Acoust. Soc. Am.* **32** 982
[6] Shariff K and Wang M 2005 *Phys. Fluids* **17** 107105
[7] Hu Z W et al 2006 *Phys. Fluids* **18** 098101
[8] Greshilov E M et al 1983 *Sov. Phys. Acoust.* **29** 275
[9] Rai M M et al 1995 *AIAA paper 95-0583*
[10] Pirozzoli S et al 2004 *Phys. Fluids* **16** 530
[11] Gao H et al 2005 *Chin. Phys. Lett.* **22** 1709
[12] Wu M and Martin P 2007 *AIAA J.* **45** 879
[13] Martin M P et al 2006 *J. Comput. Phys.* **220** 270